The Impact of Dopant Diffusion on Random Dopant Fluctuation in Si Nanowire FETs: A Quantum Transport Study

Jaehyun Lee
School of Engineering
University of Glasgow
Glasgow, United Kingdom
Jaehyun.Lee@glasgow.ac.uk

Salim Berrada
School of Engineering
University of Glasgow
Glasgow, United Kingdom
Salim.Berrada@glasgow.ac.uk

Hamilton Carrillo-Nunez
School of Engineering
University of Glasgow
Glasgow, United Kingdom
Hamilton.Carrillo-Nunez@glasgow.ac.uk

Cristina Medina-Bailon
School of Engineering
University of Glasgow
Glasgow, United Kingdom
Cristina.MedinaBailon@glasgow.ac.uk

Fikru Adamu-Lema
School of Engineering
University of Glasgow
Glasgow, United Kingdom
Fikru.Adamu-Lema@glasgow.ac.uk

Vihar P. Georgiev
School of Engineering
University of Glasgow
Glasgow, United Kingdom
Vihar.Georgiev@glasgow.ac.uk

Asen Asenov
School of Engineering
University of Glasgow
Glasgow, United Kingdom
Asen.Asenov@glasgow.ac.uk

***Abstract*—In this work, we perform statistical quantum transport simulations with 3×3 nm^2 Si nanowire (NW) field-effect transistors (FETs) to investigate the impact of dopant diffusion on random dopant fluctuation. First, we use an effective mass Hamiltonian for the transport where the confinement and transport effective masses are extracted from the tight-binding band structure calculations. The dopant diffusion along the transport direction from the source/drain regions to the channel region is modeled by the Gaussian doping profile. To generate random discrete dopants, we adopt a rejection scheme considering the 3-dimensional atomic arrangement of the NW structures. Our statistical simulation results show that the diffused dopants into the channel region cause large variability problems in Si NW FETs.**

***Keywords*—random discrete dopants, non-equilibrium Green's function, silicon nanowire, dopant diffusion, tight-binding**

I. INTRODUCTION

According to the report from the International Roadmaps for Devices and Systems (IRDS) [1], the technology generation of logic devices in industry is expected to reach 5 and 3 nm in the years 2021 and 2024, respectively. It is also predicted that in 2019, the multi-gate nanowire field-effect transistors (NW FETs) will begin to replace FinFETs due to their superior electrostatic integrity [1, 2].

In the sub-10 nm devices, the quantum transport simulations are imperative to describe the source-to-drain direct tunneling current [3, 4]. Moreover, it was reported that the quantum confinement effects in NW structures decreases both the electron and the hole mobilities [5]. Thus, employing proper Hamiltonian through the calibration of the effective masses is essential for transport simulations in Si NW FETs.

This work was supported by the European Union's Horizon 2020 research and innovation programme under grant agreement No 688101 SUPERAID7.

The significant variation associated with the random discrete dopants (RDDs) has been studied in bulk and nanoscale metal oxide semiconductor FETs (MOSFETs) during last few decades [6-8]. In 2011, Martinez *et al.* showed that Si NWFETs suffer from the random dopant fluctuation (RDF) due to their small cross-sectional area [8]. Moreover, it is difficult to avoid dopant diffusion during the thermal annealing processes [9, 10].

In this work, we perform statistical variability simulation study based on the Non-Equilibrium Green's Function (NEGF) formalism to investigate RDF in Si NWFETs with different Gaussian doping profiles which describe the dopant diffusion from the source/drain regions to the channel region. From this Gaussian doping profile, we generate RDDs by applying a rejection scheme [11]. The paper is organized as follows. Section II presents the multi-scale simulation approach including the calculation of effective masses. In Section III, we discuss our statistical quantum transport simulations of Si NW FETs having the Gaussian doping profiles with the different standard deviations. Finally, we draw the summary and conclusions in Section IV.

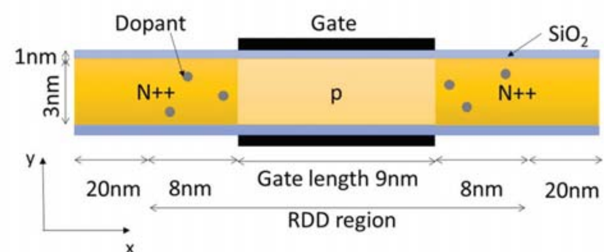

Fig. 1. Schematic diagram of the 3×3 nm^2 square Si NWFETs. The channel is surrounded by the metal gate.

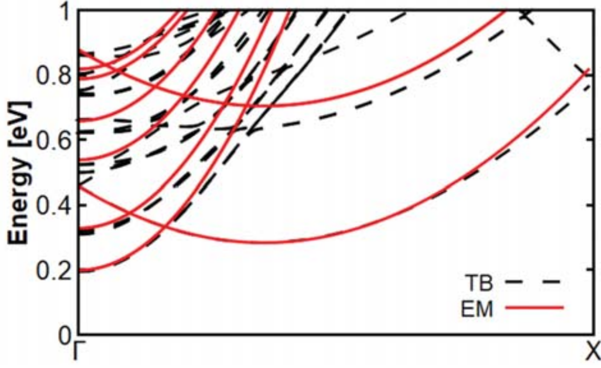

Fig. 2. Calculated conduction band structures of 3×3 nm^2 Si NW by tight-binding (TB) and effective mass (EM) methods, respectively. The conduction band edge of bulk Si is set to 0.0 eV.

II. Simulation Approach

Fig. 1 shows the schematic diagram of the n-type gate-all-around Si NW FETs simulated in this work. The devices have a 3×3 nm^2 square cross-section. The source/drain length, the gate length and the effective oxide thickness are 28 nm, 9 nm and 1 nm, respectively. The 20 nm-long source/drain regions with uniformly distributed dopants ensure good convergence. RDDs are located in the remaining 8 nm-long source/drain regions adjacent to the gate and in the channel region. The doping concentrations in the channel and the source/drain regions are 10^{15} (p-type) and 10^{20} (n-type) cm^{-3}, respectively. The work-function of the metal gate and the source-to-drain bias (V_{DS}) are set to 4.55 eV and 0.6 V, respectively. The transport direction in all simulated devices is [100].

A. Calculations of the effective masses of the Si NW

We calculate the band structure of the [100]-oriented 3×3 nm^2 Si NW by using the $sp^3d^5s^*$ tight-binding (TB) method, with Boykin's parameter set [12], implemented in QuantumATK from Synopsys Quantumwise [13]. Based on the conduction band shown in Fig. 2, we calculate the transport and confinement effective masses. The former can be obtained through the equation:

$$m^* = \hbar^2 \left(\frac{\partial^2 E}{\partial k^2}\right)^{-1} \quad (1)$$

where $\hbar$ is the reduced Planck constant, E is the energy, and k is the wave vector along the transport direction. For the latter case, we find appropriate values to reproduce the first and the second conduction sub-band energies. As a result, the band structure from effective mass (EM) Hamiltonian is in good agreement with that from TB Hamiltonian (see Fig. 2).

B. Transport simulations with RDDs

We solve the Poisson and the coupled mode-space NEGF transport equations [14] self-consistently to calculate the electron density and the current in the device (see Fig. 1). This simulation environment is implemented in the Glasgow Nano-Electronic Simulation Software (NESS) [15]. The doping profiles of source/drain regions are modeled by the Gaussian distribution function which describes dopant diffusion by the

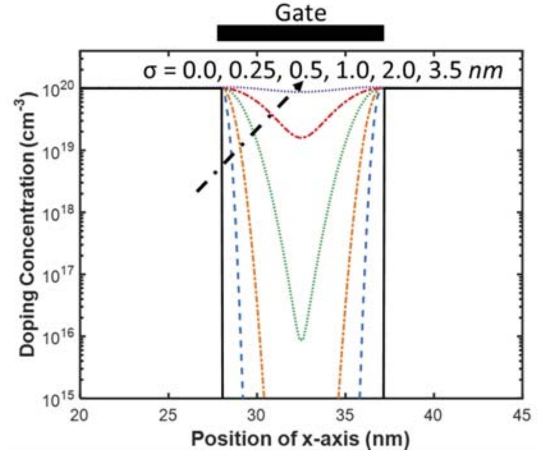

Fig. 3. Doping profiles along the transport direction (see Fig. 1) of Si NWFETs with different σ values .

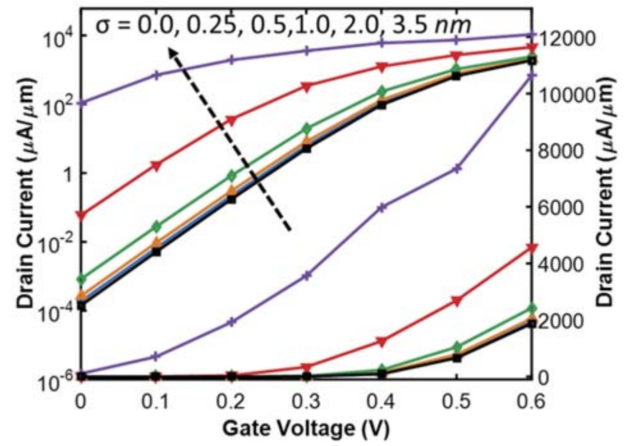

Fig. 4. I_D-V_G characteristics of devices having the different Gaussin doping profiles without RDDs.

post-thermal annealing processes. The standard deviation σ in the Gaussian doping profile is related to the diffusion length and can be defined as below [9, 10]:

$$\sigma = \sqrt{2Dt} = \sqrt{2 \times D_0 \exp\left(-\frac{E_a}{k_B T}\right) t} \quad (2)$$

where D is the diffusion coefficient, t is the diffusion time, D_0 is the typical diffusion coefficient of the dopant, E_a is the activation energy of the dopant, k_B is the Boltzmann constant, and T is the temperature. As T increases and/or t increases, the diffusion length increases.

Fig. 3 illustrates the doping profiles of the simulated devices in this work. We have considered six different σ values. When σ is 0.0 nm, there is no sub-diffusion of dopants under the gate. Moreover, as σ increases, the effective channel length decreases, and when we reach the limit σ = 3.5 nm, the metallurgical junctions disappear.

RDDs are generated by a rejection scheme considering the atomic arrangement in the Si NW structure with lattice

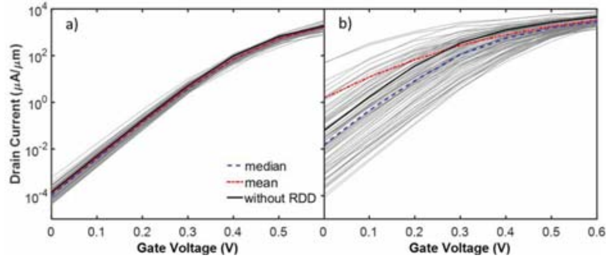

Fig. 5. I_D-V_G characteristics when a) σ = 0.0 nm and b) σ = 2.0 nm. The result with the continuous doped device (solid line) and median (dashed line) and mean (dotted line) values of devices with RDDs are also presented.

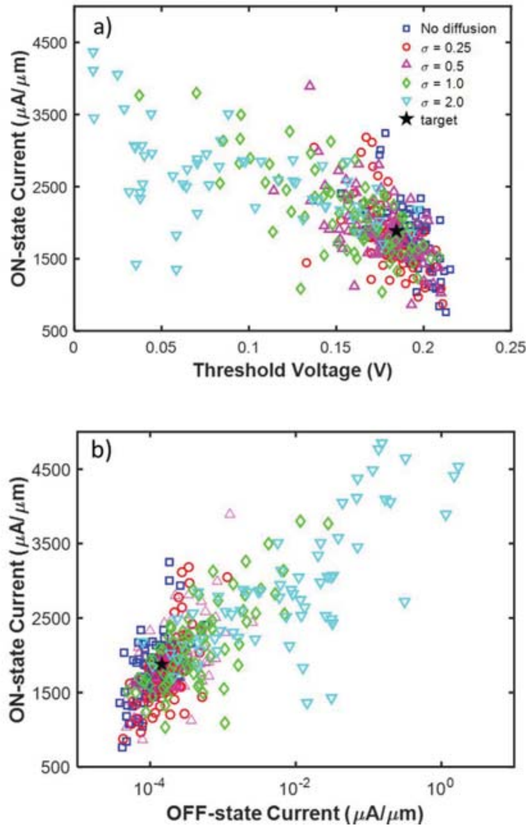

Fig. 6. a) V_{TH} versus I_{ON} and b) I_{OFF} versus I_{ON} with different doping profiles.

parameter of 5.43 Å [11]. Thus, the number of dopants in the RDD region follows the Poisson distribution. We have simulated 100 devices for each σ and ensembles of approximately 84 well-converged devices are considered for the statistical analysis in this work.

III. SIMUALTION RESULTS AND DISCUSSION

Fig. 4 shows the drain current (I_D) – gate voltage (V_G) characteristics of devices having the different Gaussian doping profiles without RDDs. Herein, I_D is normalized by the width of the NW (3 nm). As σ increases, the ON-state current (I_{ON}) and the OFF-state current (I_{OFF}) increase significantly. I_{ON} and I_{OFF} are defined at $V_G = V_{DS}$ = 0.6 V and V_G = 0.0 V, respectively. We have also found that σ should be less than 1.0 for I_{OFF} to be less than 10 nA/μm, which is the criteria for the high-performance devices remarked in the IRDS report [1].

TABLE I. THE YEILD OF DEVICES WITH THE DIFFERENT GAUSSIAN DOPING PROFILES.THE MARGIN TO THE TARGET VALUES IS SET TO 25 %. WE HAVE CALCULATED THE YEILDS FOR I_{ON}, I_{OFF}, V_{TH}, AND THE THREE PARAMETERS, RESPECTIVELY.

σ values	I_{ON}	I_{OFF}	V_{TH}	I_{ON}, I_{OFF} and V_{TH}
0.0	82.95 %	81.82 %	100.00 %	64.77 %
0.25	83.13 %	53.01 %	97.59 %	39.76 %
0.5	93.33 %	43.33 %	96.67 %	37.78 %
1.0	95.12 %	25.61 %	75.61 %	20.73 %
2.0	98.80 %	2.41 %	20.48 %	2.41 %

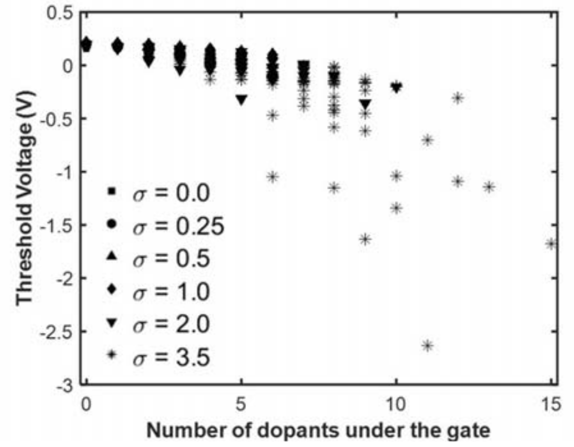

Fig. 7. V_{TH} versus the number of n-type dopants in the channel region. The all the simulated data of devices with σ = 0.0, 0.25, 0.5, 1.0, 2.0, and 3.5 nm is taken into account.

The I_D–V_G characteristics of devices with RDDs when their σ values are 0.0 and 2.0 nm are shown in Figs. 5a) and b), respectively. We have considered 88 and 83 well-converged devices, respectively. The mean and median values of the drain current are also drawn in these figures. It is important to note that devices with σ = 2.0 nm have much larger variability than that with σ = 0.0 nm in terms of I_{OFF}, I_{ON}, and threshold voltage (V_{TH}). Additionally, the big difference between the mean and median values of I_{OFF} is observed when σ = 2.0 nm.

Fig. 6 illustrates correlation plots between I_{ON} and V_{TH}, and between I_{ON} and I_{OFF}. Herein, V_{TH} is defined as V_G when I_D is 100 nA/μm. The star symbol in these figures indicates the target value, which is obtained from the simulated device with σ = 0.0 nm and continuous doping profile (see the black-square curve in Fig. 4). In Fig. 6a), it is found that as V_{TH} decreases, I_{ON} increases. Moreover, a strong correlation between $log(I_{OFF})$ and I_{ON} is observed as shown in Fig. 6b). The important finding in Fig. 6 is that the bigger σ becomes, the larger variability problems are. This observation is in good agreement with the results in Fig. 5.

Furthermore, we have calculated the yield associated with RDF in terms of I_{ON}, I_{OFF}, and V_{TH}. The margin to the target values (see the star symbols in Figs. 6 a) and b)) is set to 25 %. The calculated yields are summarized in Table I. When only I_{ON} is taken into account, the yield increases with the large σ value, and it is in good agreement with the results shown in Fig. 4. However, considering I_{OFF} and V_{TH}, the yield decreases dramatically as the σ value increases. Therefore, the total yield (see the last column in Table I) with $\sigma = 0.0$ nm is 65%, while the yield with σ = 2.0 nm is only 2%. It is highlighted that the increase of I_{OFF} and the V_{TH} variation due to diffusion of dopants are dominant compared to the I_{ON} variation.

The dependence of V_{TH} on the number of diffused dopants into the channel region is shown in Fig. 7. This figure represents all the simulation results with different σ values and RDDs performed in this work. As we expected, more number of dopants are positioned under the gate with the large value of σ. We also notice that the significant V_{TH} variation and decrease of V_{TH} are due to the increase number of diffused dopants into the channel region. This behavior is in consonance with the results in Table I.

IV. CONCLUSIONS

We have performed statistical quantum transport simulations to investigate the random dopant fluctuation in Si nanowire FETs. Different doping profiles are taken into account to describe the dopant diffusion from the source/drain regions in the channel region due to the post-thermal annealing processes. We have found that as the diffusion length increases, e.g with higher annealing temperature and/or longer annealing time, the variability problems in terms of the OFF-state current and the threshold voltage become more significant. Therefore, decreasing the thermal budget during the fabrication is important to solve the variability problem.

REFERENCES

[1] International Roadmaps for Devices and Systems [online]. Available at https://irds.ieee.org/ [Accessed June 29, 2018].

[2] Y. Cui, Z. Zhong, D. Wang, W. U. Wang, and C. M. Lieber, “High Performance Silicon Nanowire Field Effect Transistors”, Nano Lett., vol. 3, no. 2, pp. 149-152, Jan. 2003.

[3] J. Wang and M. Lundstrom, “Does source-to-drain tunneling limit the ultimate scaling of MOSFETs?”, in IEDM Tech. Dig., 2002, pp. 707-710.

[4] H. Kawaura, T. Sakamoto, and T. Baba, “Observation of source-to-drain direct tunneling current in 8 nm gate electrically variable shallow junction metal–oxide–semiconductor field-effect transistors”, Appl. Phys. Lett., vol.76, pp. 3810-3812, Apr. 2000.

[5] R. Rhyner and M. Luisier, “Phonon-limited low-field mobility in silicon: Quantum transport vs. linearized Boltzmann Transport Equation”, J. Appl. Phys., vol. 114, pp. 223708, Dec. 2013.

[6] A. Asenov, “Random dopant induced threshold voltage lowering and fluctuations in sub-0.1 fjim MOSFET's: A 3-D "atomistic" simulation study”, IEEE Trans. Electron Devices, vol. 45, no. 12, pp. 2505-2513, Dec. 1998.

[7] Y. Li, H. Chang, C. Lai, P. Chao, C. Chen, “Process Variation Effect , Metal-Gate Work-Function Fluctuation and Random Dopant Fluctuation of 10-nm Gate-All-Around Silicon Nanowire MOSFET Devices”, in IEDM Tech. Dig., 2015, pp. 887-890.

[8] A. Martinez, M. Aldegunde, N. Seoane, A. R. Brown, J. R. Barker, and A. Asenov, “Quantum-transport study on the impact of channel length and cross sections on variability induced by random discrete dopants in narrow gate-all-around silicon nanowire transistors”, IEEE Trans. Electron Devices, vol. 58, no. 8, pp. 2209-2217, Aug. 2011.

[9] A. Fick, “Ueber Diffusion”, Annalen der Physik, vol. 94, pp. 59-86, 1885.

[10] R. C. Jaeger, “Introduction to Microelectronic fabrication”, 2nd edition, Prentice Hall, 2002.

[11] D. J. Frank, Y. Taur, M. Ieong, H.-S.P. Wong, “Monte Carlo Modeling of Threshold Variation due to Dopant Fluctuations”, 1999 Symp. VLSI Tech. Dig., pp. 169-170.

[12] T. B. Boykin, G. Klimeck and F. Oyafuso, “Valence band effective-mass expressions in the sp3d5s* empirical tight-binding model applied to a Si and Ge parametrization.”, Phys. Rev. B, vol. 69, pp. 115201, Mar. 2004.

[13] QuantumATK version 2017.2, Synopsys QuantumWise A/S. Available at http://www.quantumwise.com [Accessed June 29, 2018]

[14] M. Luisier, A. Schenk, and W. Fichtner, “Quantum transport in two- and three-dimensional nanoscale transistors: Coupled mode effects in the nonequilibrium Green’s function formalism”, J. Appl. Phys., vol. 100, pp. 043713, June 2006.

[15] S. Berrada, H. Carrillo-Nuñez, J. Lee, C. Medina-Bailon, T. Dutta, M. Duan, F. Adamu-Lema, V. Georgiev, and A. Asenov, “NESS: new flexible Nano-Electronic Simulation Software”, in Proc. SISPAD 2018.